Computers and Electronics in Agriculture 135 (2017) 222–232

Contents lists available at ScienceDirect

Computers and Electronics in Agriculture

journal homepage: www.elsevier.com/locate/compag

Original papers

Quantifying time-series of leaf morphology using 2D and 3D photogrammetry methods for high-throughput plant phenotyping

Nan An [a,*], Stephen M. Welch [a], R.J. Cody Markelz [b], Robert L. Baker [c], Christine M. Palmer [b], James Ta [b], Julin N. Maloof [b], Cynthia Weinig [c]

[a] Department of Agronomy, Kansas State University, Manhattan, KS 66506, USA
[b] Department of Plant Biology, University of California Davis, Davis, CA 95616, USA
[c] Department of Botany, University of Wyoming, Laramie, WY 82071, USA

ARTICLE INFO

Article history:
Received 13 May 2016
Received in revised form 11 January 2017
Accepted 4 February 2017
Available online 24 February 2017

ABSTRACT

Conventional phenotyping methods impose a significant bottleneck to the characterization of genotypic and environmental effects on trait expression in plants. In particular, invasive and destructive sampling methods along with manual measurements widely used in conventional studies are labor-intensive, time-consuming, costly, and can lack consistency. These experimental features impede large-scale genetic studies of both crops and wild plant species. Here, we present a high-throughput phenotyping pipeline using photogrammetry and 3D modeling techniques in the model species, *Arabidopsis thaliana*. We develop novel photogrammetry and computer vision algorithms to quantify 2D and 3D leaf areas for a mapping population of 1050 *Arabidopsis thaliana* lines, and use 2D areas to analyze plant nastic movements and diurnal cycles. Compared to the 2D leaf areas, 3D leaf areas show an uncorrupted growth trend regardless of plant nastic movement. With optimized algorithms, our pipeline throughput is very computationally efficient for screening a large number of plants. The pipeline not only supports measurement of organ-level growth and development over time, but also enables analysis of whole-plant phenotypes and, thus, identification of genotype-specific performance. Further, the accuracy results evaluating the relationship between physical dimensions and 3D measurements indicate an $R^2 = 0.99$, and the average 3D area processing time per plant is 0.02 s. Our algorithms provide both high accuracy and throughput in plant phenotyping, thereby, enabling progress in plant genotypic modeling.

Published by Elsevier B.V.

1. Introduction

Interest in high-throughput plant phenotyping approaches has increased in recent years (Fiorani and Schurr, 2013). Automated approaches to measure traits will improve the efficiency and accuracy of plant phenotyping, which is critical to understanding how genetic and environmental factors are linked to plant phenotypes (Furbank and Tester, 2011; Fiorani and Schurr, 2013; Kjaer and Ottosen, 2015). Studies seeking to characterize the genetic basis of complex traits through either genome-wide association analyses or quantitative trait locus (QTL) mapping depend, for instance, on trait measurements in hundreds to thousands of replicate plants (Clarke et al., 1995; Brachi et al., 2010). With the advent of next-generation sequencing approaches, it is the rate of phenotyping rather than marker development that now imposes the upper limit on the size of mapping experiments. Various sensors, such as 3D laser scanning sensors, RGB/near-infrared cameras, hyperspectral sensors, thermal imaging systems, and chlorophyll fluorescence imaging sensors, have recently been integrated into automated phenotyping pipelines to estimate plant phenotypic traits in mapping populations (Rascher et al., 2011; Mahlein et al., 2012). Here, we develop approaches and analyses for high-throughput phenotyping of leaf morphological traits.

Leaf morphological features can be important determinants of plant performance, because leaf size and shape influence photosynthesis, stomatal conductance, and transpiration efficiency (Juenger et al., 2005). Previous studies used imaging systems with commercial or customized software to acquire areas of single leaves and rosettes from 2D images (Candela et al., 1999; Pérez-Pérez et al., 2002; Bylesjö et al., 2008; Weight et al., 2008; Backhaus et al., 2010; Ali et al., 2012; Maloof et al., 2013; Easlon and Bloom, 2014). Invasive and destructive plant sampling methods (e.g., harvesting plant leaves) were used in these studies during image acquisition. Such methods have the disadvantage of precluding multiple measurements on a given replicate. In addition, they are highly labor-intensive due to the large number of plants needed for repeated harvests and the amount of manual work.

* Corresponding author.
E-mail address: an_198317@hotmail.com (N. An).

http://dx.doi.org/10.1016/j.compag.2017.02.001
0168-1699/Published by Elsevier B.V.

2D imaging techniques can provide useful phenotypic information, such as estimates of rosette area or time-series data of leaf nastic movements that are indicative of circadian rhythms. Mullen et al. (2006) used image processing software to manually measure leaf inclination angle and study leaf movements over short intervals. Hong et al. (2013), Dornbusch et al. (2014) and Greenham et al. (2015) used imaging systems to track leaf tip movements and estimate leaf inclination angles as a proxy for circadian cycles. These studies all reveal that nastic movements occur on 24-h diurnal cycles. However, leaf tip tracking from a side view does not allow for simultaneous detection of leaf areas that change due to growth. On the other hand, nadir-looking views that detect area will only be accurate once per day, when nastic movements reach an angle perpendicular to the line of sight. Leaf area and plant canopy measurements based on 3D plant structure can resolve these limitations and provide both good size estimates (regardless of plant nastic movements) as well as time-series data necessary for estimates of circadian rhythms.

Modeling and analyzing plant 3D shape is a computationally-intensive and time-consuming process (Paulus et al., 2014; Vos et al., 2009; El-Omari and Moselhi 2011). Typically, there are two types of sensors used for plant 3D modeling: active sensors and passive sensors. Laser sensors such as LIDAR (Light Detection And Ranging) are active sensors for sensing plant 3D shapes. They emit a laser beam, and the time it takes for the reflected light to return to the sensor is used to compute a depth map or generate a 3D point cloud of the plant canopy. Point clouds are simply sets of 3D coordinates that, collectively, have the shape of the object of interest. None of the points are connected, so phenotypes of interest have to be inferred using complex algorithms.

Palacín et al. (2007) used a laser sensor to scan pear trees and estimate canopy surface; Hosoi and Omasa (2009) utilized portable LIDAR imaging technology to model tomato plant canopy in a three-dimensional space; Keightley and Bawden (2010) used ground-level LIDAR to estimate plant biomass. Coarse 3D measurements were sufficient for the aims of these studies, but detailed plant structures could not be quantified from the 3D models. Furthermore, the 3D measurements of these studies were not collected using an automated pipeline. Only limited numbers of plants could therefore be analyzed during the growth period—too few for studies seeking to quantitatively relate genotypes to phenotypes within dynamic environments (Granier et al., 2006; Berger et al., 2010; Hartmann et al., 2011). On the other hand, Kjaer and Ottosen 2015 used the commercial 3D laser triangulation scanner PlantEye F300 to automate plant growth measurement. This technology improves spatial and temporal resolution for higher throughput plant phenotyping using a laser sensor.

In recent years, an increasing number of studies have used the LIDAR-based LemnaTec Scanalyzer HTS system (http://www.lemnatec.com) to obtain 3D point clouds. This system includes an automated analysis pipeline that can extract a number of phenotypic traits (Green et al., 2012; Chen et al., 2014; Dornbusch et al., 2014). However, the cost of the system presents a significant impediment for many smaller research laboratories and institutions.

Microsoft Kinect (https://www.microsoft.com/en-us/kinectforwindows/) is a low-cost sensor originally designed for computer gaming, whose operation is based on time-of-flight measurements for a raster pattern of infrared beams. It has become a very popular choice for modeling 3D shapes in the robotic and computer vision communities. Some studies have evaluated its utility in plant phenotyping (Chéné et al., 2012; Azzari et al., 2013; Paulus et al., 2014). There are, however, several drawbacks. The throughput using Kinect is relatively low, and therefore not suitable for high-density time-series phenotyping of mapping populations. Additionally, its laser beams are not bright enough for outdoor daytime use (Azzari et al., 2013). Data can be acquired during the night, but doing so is biologically problematic as the laser wavelength of the first Kinect model falls within the phytochrome absorption band. Phytochromes are highly sensitive photoreceptors with many roles in the control of plant processes so exposure to the laser could, in principle, elicit undesired phenotypic responses. The recently-released second Kinect model uses a longer wavelength that falls outside of known photoreceptor sensitivity bands.

The second approach is to use passive sensors—in particular, digital cameras—along with photogrammetric techniques to capture 3D models of plants. The major advantage of these techniques is that because they are based on images, they can produce much more detailed information about the surface features being imaged and much faster data acquisition and process rate than laser-based scanning. This information is contained in a *texture image* that is painted onto the 3D model when it is displayed. Furthermore, because a texture image *is* an image, it can be subjected to common image processing techniques to extract phenotypic information of interest. Finally, digital cameras can be much less expensive than laser-based active sensors like LIDAR.

Previous photogrammetry work includes that of Quan et al. (2006) and Tan et al. (2007), who used the techniques to estimate camera positions and produce point clouds, but did not extract any phenotypes. Quan et al. (2006) proceeded beyond point clouds, combining clustering, image segmentation, and polygon models to create 3D canopy models. These were, however, of very coarse resolution. Biskup et al. (2007) developed a stereo imaging system using two digital cameras to model soybean plants in a three-dimensional space. This, too, was a point cloud approach, but they went on to produce false-color images of leaf angle. Santos and Oliveira (2012) used stereo imaging system with photogrammetric and computer vision algorithms to generate 3D models of plants, but, as above, did not extract phenotypes. While the preceding studies produced 3D plant canopy models, they used a small number of cameras whose positions and orientations were changed to capture different viewing angles. Although only requiring a few cameras is an advantage, the resulting low throughput does not permit highly time-resolved studies for the large number of plants used in mapping populations.

In this study, we first demonstrate an analysis using an indoor imaging pipeline to extract time-series 2D rosette areas of a mapping population of 1050 *Arabidopsis thaliana* lines from images for studying plant nastic movement, diurnal cycles, and plant growth. We then used the pipeline to generate 10-day time-series of 3D models with a one-hour temporal resolution for the same plant population. Sequentially, the pipeline color and optical distortion corrects RAW images of potted plants on growth chamber shelves, generates 3D models of half-shelf areas, segments individual plants, pairs them with their genotypes, and then extracts time-series data of leaf growth and movement.

2. Materials and methods

2.1. Imaging acquisition system

The imaging acquisition process used the same indoor pipeline described in a previous study (An et al., 2016), to measure shade-avoidance responses in a nested association mapping (NAM) population of *Arabidopsis thaliana*. In this study, 108 Canon Powershot S95 cameras were mounted on six 0.80-by-2.13-m frames facing straight down on six shelves that received two different lighting treatments (Fig. 1). On each shelf, 18 cameras were mounted in a 2-row stationary camera frame at a 0.4-m height and photographed 24 4-by-4 pot flats hourly. A modified intervalometer script with Canon Hack Development Kit (CHDK) firmware trig-

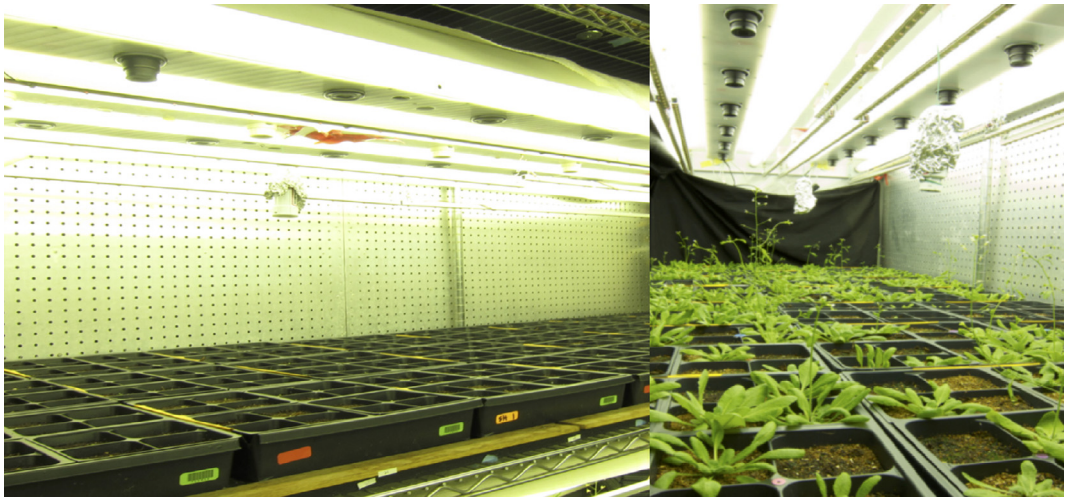

Fig. 1. Imaging acquisition system. The 18 cameras were mounted in two rows on each shelf. All of the cameras were pointed straight down as nadir viewing angle.

gered the cameras simultaneously at the beginning of each hour. In order to ensure all images had at least 50-percent overlap, the focal length of the cameras was set at 28 mm (35 mm equivalent) to maximize the field-of-view (FOV). Daytime (5:00 am–8:00 pm) images were stored and transferred to a local data server and processed for subsequent analyses. The RAW image file format was selected for preserving all image metadata.

2.2. 2D rosette analysis

2.2.1. Image pre-processing, orthophoto generation, single-plant extraction, and genotype assignment

The first processing steps used the automated high-throughput phenotyping pipeline introduced in An et al., 2016. Briefly, the Canon Digital Photo Professional (DPP) program and a customized color-grid vinyl poster were used for RAW image color correction, optical distortion correction, and TIFF conversion. The converted TIFF images were imported into the Agisoft Photoscan Pro (Photoscan) program (http://www.agisoft.com) to generate an orthophoto for each shelf for correcting perspective distortion, so that each pixel of an orthophoto was being viewed straight down and the pixel size of the orthophoto was 0.1 mm.

Each orthophoto was first segmented to a plant-only binary image using the Normalized Green–Red Difference Index (NGRDI) (Hunt et al., 2005) and the Otsu threshold method to eliminate non-plant pixels. In a parallel step, the orthophoto was segmented to detect the pot edges, which aided in the isolation of replicates plants. Segmentation was augmented by use of the probabilistic Hough Transformation to search for pot edges. The output of these steps was a set of coordinate grids delineating pot edges.

The pots were tracked during the entire growth period using a customized color dot system, during which they were periodically repositioned to randomize any effects of location within the growth chamber. Based on records made at planting, the genotype of each plant was assigned to its grid cell. Lastly, single plant binary images, each with its known genotype, were extracted from the grid cells. The detail of the processes discussed above were presented in An et al. (2016)

2.2.2. 2D rosette area analysis for plant nastic movement and diurnal cycle analysis

Plant 2D rosette area in each plant-only binary image can be simply calculated by computing the total number of white pixels in each single-rosette binary image. In this study, we tracked one plant during a 10-day growth period and used the Fourier Transform to study the characteristics of plant nastic movements. The hourly 2D rosette area values of the plant were calculated during this 10-day period. Because of the experimental design of the chamber study, no image data were collected during the night (9:00 pm–5:00 am). In order to extract the characteristics of the growth pattern, a linear interpolation algorithm was applied to estimate the rosette area for night hours. The Savitzky–Golay filter was utilized in the following step to yield a smoothed growth curve and minimize possible noise in the rosette area measurements. A third degree Savitzky–Golay filter was used to prevent curve oversmoothing. In order to reveal the 2D rosette area oscillation caused by the nastic movements, the Matlab detrend algorithm (http://www.mathworks.com/help/matlab/ref/detrend.html) was used to eliminate the ascending growth trend from the smoothed 10-day 2D rosette area curve. The Fourier Transform was then applied to the resulting data to study the diurnal cycle.

2.3. 3D rosette analysis

2.3.1. Camera array calibration and shelf-based 3D mesh generation

Camera calibration is the process of determining which light beam excites a given pixel of the image sensor (Bellasio et al., 2012). This entails solving for two sets of numbers. *Intrinsic parameters* specify the optical behavior of the camera itself. *Extrinsic parameters* tell where the camera is positioned in space and the direction that it is pointing. Intrinsic parameters are often determined one camera at a time using special targets and software; however, this was not feasible due to the large number of cameras in this study. Instead, the two-row camera array of each shelf was calibrated as one imaging system using Photoscan's built-in camera calibration function.

The customized color-grid poster was printed on a shelf-size (0.80 m × 2.13 m) vinyl panel, which was mounted and stretched flat on each shelf surface before the experiment started. The poster was photographed by the 18-camera array of each shelf. After preprocessing by DPP, all 18 images were imported into Photoscan to build a sparse point cloud and a dense point cloud (Fig. 2). Photoscan first estimated camera intrinsic parameters, including the image dimension in pixels, the focal length, and the coordinates of the pixel intersected by the optical axis. Other intrinsic parameters estimated by Photoscan describe the radial and tangential lens distortion. Because early experience showed that Photoscan

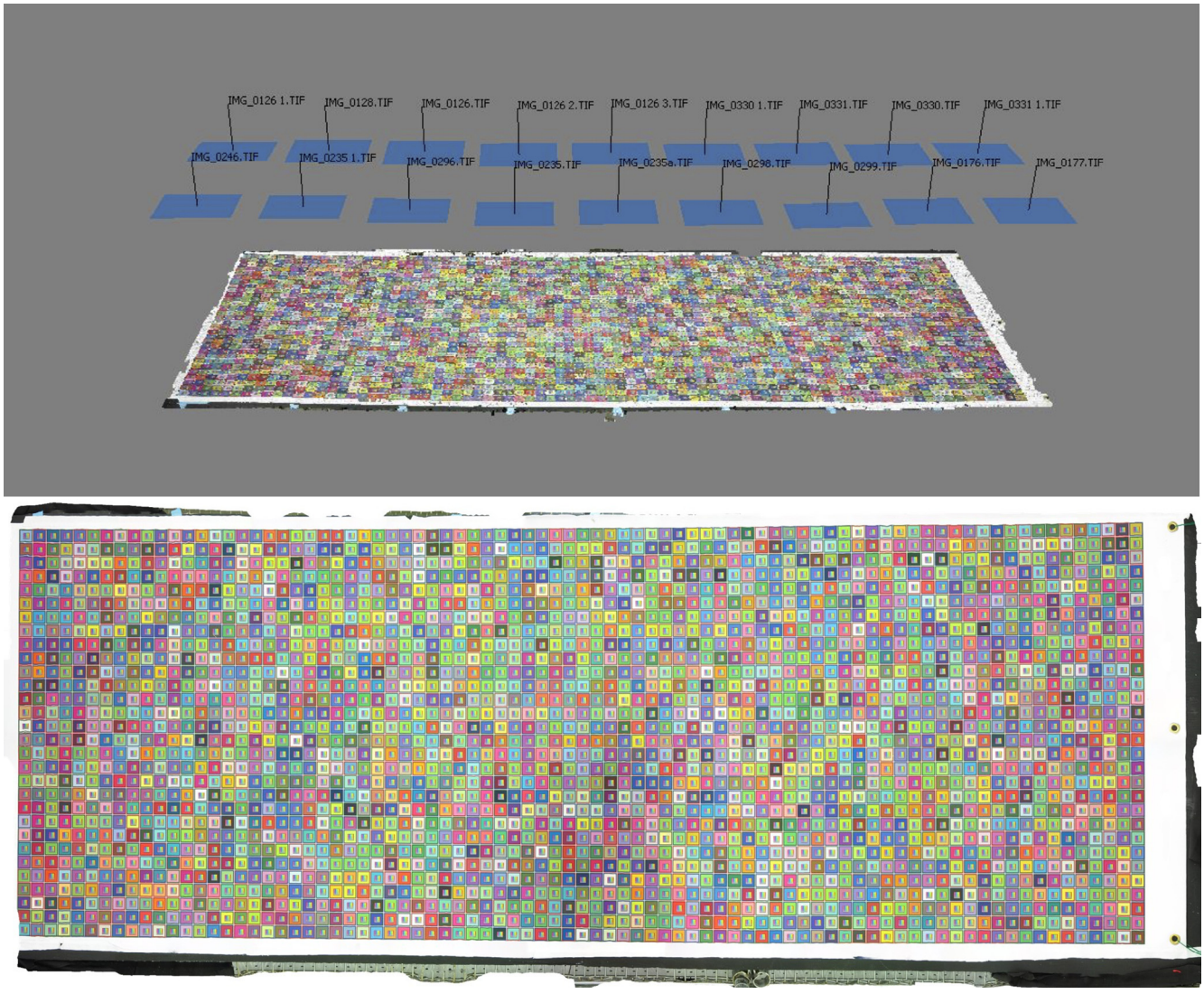

Fig. 2. Camera calibration. The dense point cloud in a three-dimensional space generated by Photoscan for calibrating a two-row camera system using a customized color-grid poster. The blue boxes are the estimated camera positions in a three-dimensional space; the black lines show the orientations of each camera. The camera intrinsic parameters were estimated by this process. The bottom image is the orthophoto of the color-grid poster generated after the calibration process.

was not fully effective at correcting lens distortion, an initial stage of lens distortion removal was first performed by DPP. An orthophoto and a 3D mesh surface of the color-grid poster were also generated by Photoscan for 3D area validation (Fig. 2).

Photoscan next calculated the extrinsic parameters that are the X, Y, and Z coordinates of each camera's focal point and the roll, pitch, and yaw angles of the optical axis. Fig. 2 shows the cloud of over four million points that Photoscan produced during the calibration process as well as a visual depiction of selected internal and external camera parameters. After ensuring the estimation errors of 18 camera positions were smaller than 0.5 pixels, all calibration parameters were exported to a camera calibration xml file that was used in all subsequent analyses.

Due to the camera sensor limitation, after plants were placed on the shelf, there was not enough image overlap between the two rows of cameras to build a 3D model for the entire shelf. Instead, half-shelf models were constructed, each from a set of nine images, along with the camera calibration data just described. The output was a file in Polygon File Format (PLY), which is a standard format for colored 3D mesh data. Fig. 3 shows a rendering of a half-shelf mesh model.

2.3.2. Single 3D plant model segmentation and plant genotype assignment

In most computer vision studies, 3D mesh segmentation is a computationally-intensive and time-consuming process. For a half-shelf 3D mesh such as the one shown in Fig. 3, there are approximately 11 million points (vertices) connected to over 23 million faces (triangles). Locating the triangles comprising individual plants within the mesh depicting all objects in the half-shelf was technically infeasible with conventional computer vision algorithms. We developed a novel, computationally-efficient method to (1) segment single-plant 3D models from the half-shelf meshes and (2) assign the corresponding genotype designations simultaneously. The key is the half-shelf PLY file exported from Photoscan and the segmented orthophoto.

There are two main sections of information contained in each PLY file. The first section contains the X, Y, Z vertex positions, unit normals (magnitude-one vectors perpendicular to the plant surface at each vertex position), and the RGB vertex colors. When the mesh is rendered, colors in between the vertices can be filled in by interpolation. Alternatively, the faces can be colored from data in a texture file, which is synthesized from the original

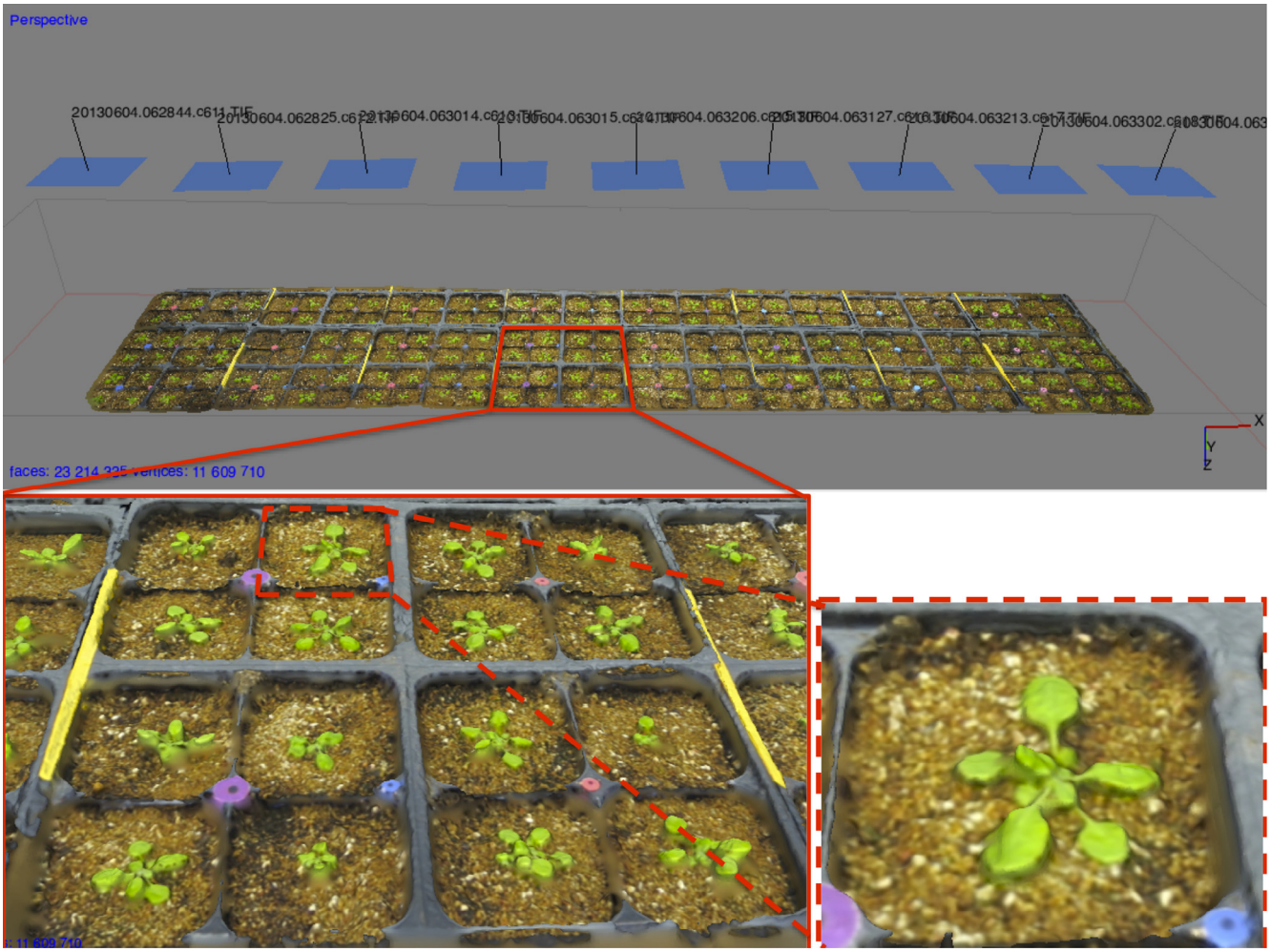

Fig. 3. A half-shelf 3D mesh generated by Photoscan. The top center is the 3D mesh generated by one-row camera array; the lower-left is a close-up view for one 4-by-4 flat; the lower right is a close-up view for one plant.

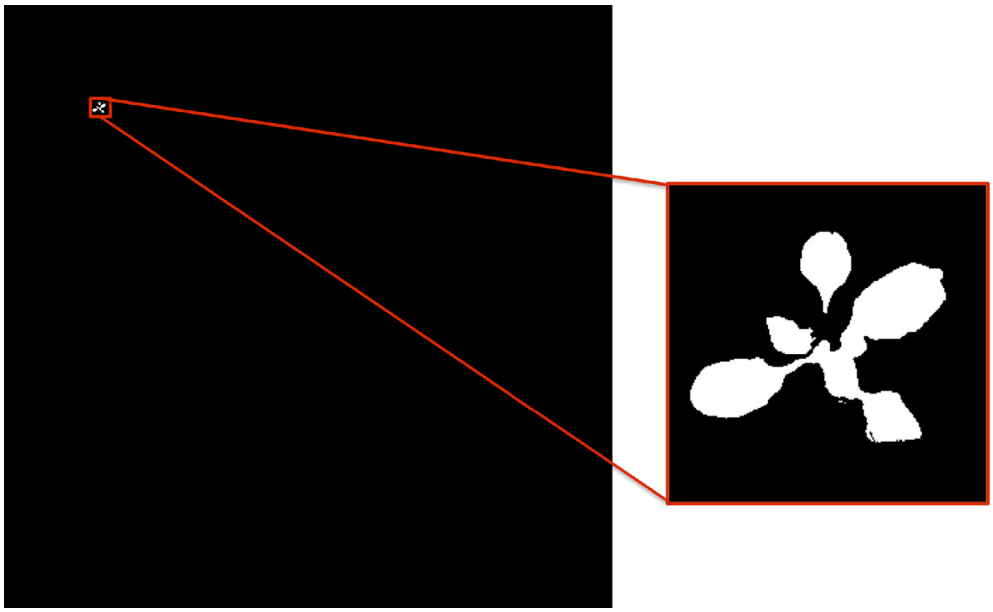

Fig. 4. Single-plant binary image for extracting a single-plant 3D model. Left: A single-plant binary image with the original orthophoto's dimension. The black area in the left image is used to eliminate the non-related mesh. Right: the close-up view of this plant.

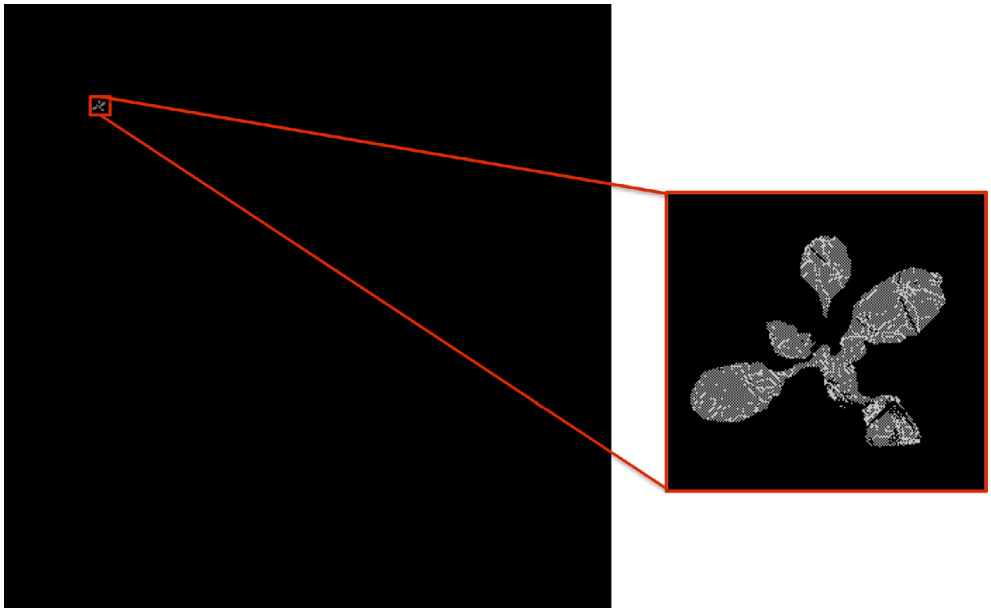

Fig. 5. A single-plant vertex map. Left: A single-plant vertex map for representing the saved vertices of the 3D mesh. The grey pixels stand for the saved corresponding vertices from the half-shelf 3D mesh. Black area means that the corresponding area on the mesh was eliminated. Right: the close-up view of this vertex map.

images. The latter option was used here because it provides more spatial detail.

The second section describes the triangular faces by listing the ID numbers for each of the three vertices that bound the triangle. Also listed are the 2D pixel coordinates where each vertex is located in the orthophoto. This builds a relationship between 3D and 2D, but the linkage is one-directional. That is, from every 3D vertex one can locate a 2D pixel, but from that 2D pixel one cannot easily locate its corresponding 3D vertex.

We located binary images for each single plant, but they were left embedded in a background that was the same size as the orthophoto (Fig. 4). Then, all the vertices in the mesh were scanned, and the colors of their corresponding orthophoto pixels were examined. Any vertex linked to a black pixel could not be a 3D point in the plant and was excluded from the orthophoto (Fig. 5). Vertices linked to the plant pixels were color-coded by the plant IDs. By using the color-coded points, the vertices and faces of each plant were efficiently sorted and then extracted from the half-shelf 3D mesh. Finally, these extracted vertices and faces were exported into one PLY file in order to generate single-plant 3D models for each plant (Fig. 6). The beauty of this process is that, because genotype information of the single-plant binary image is assigned during its extraction, the genotype of the 3D model is automatically known. Since the 3D mesh has much finer resolution than 2D texture image, the 3D mesh segmentation in Fig. 6 shows some rough edges.

2.3.3. 3D area measurement for a single plant

To estimate the area of the plant, it is only necessary to sum the areas of the triangular faces of which its 3D model is composed.

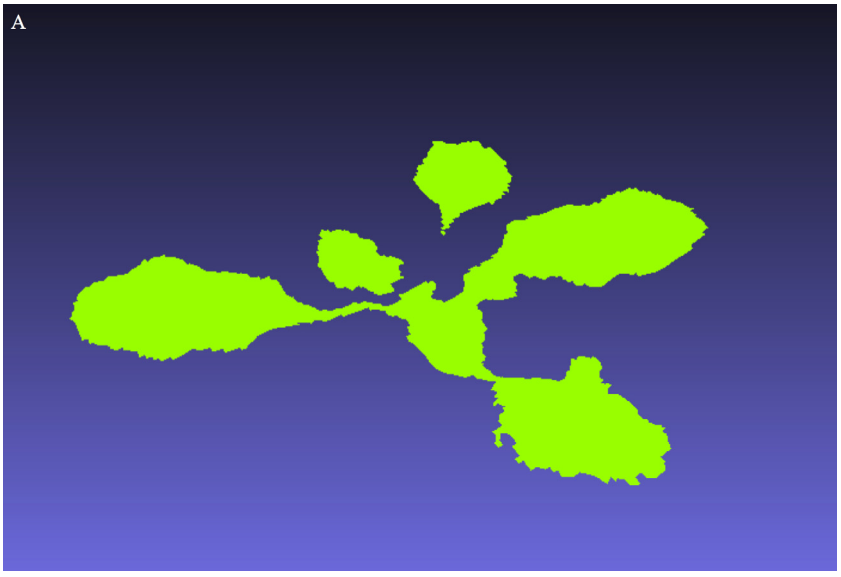

Fig. 6. A single-plant 3D model. The extracted single-plant 3D model generated by using its segmented orthophoto. The rough leaf edges are due to the spatial resolution difference between the orthophoto and the 3D mesh.

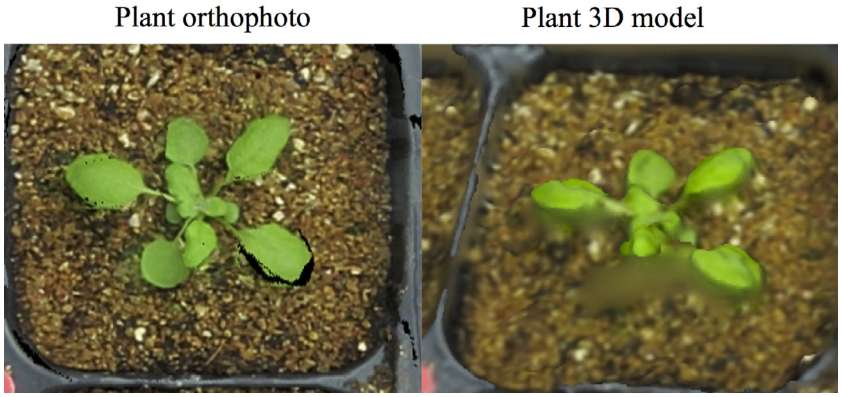

Fig. 7. Plant orthophoto compared to 3D model. One sample plant was analyzed in this article. The left image is the orthophoto of this plant, and the right image is its 3D model before single-plant 3D model extraction. The black area in the left Fig. is the stitching artifacts due to high leaf curvature after orthophoto generation process.

The area of each face was computed by: (1) converting its three vertices (A, B, and C) into two vectors, *AB* and *AC*, (2) calculating the magnitude of the cross product of these two vectors, which equals the area of a parallelogram having these two vectors as sides, and 3) the face area is half of this parallelogram's area.

2.3.4. Comparison between time-series 2D and 3D rosette areas

In order to compare rosette areas extracted based on 2D images and 3D models, a plant (Fig. 7) was tracked during a 10-day growth period, and both its 2D and 3D areas were calculated every hour. Because no images were collected from 9:00 pm to 5:00 am each day, linear interpolation was used to estimate rosette area overnight. Then, the Savitzky–Golay filter was applied to yield a smoothed growth curve. Because the 2D and 3D systems had different units (pixel and mesh coordinates, respectively), the two areas could not be compared directly. Therefore, the values were converted to Z scores on a daily basis and plotted together for comparison. This statistical analysis was implemented in Matlab.

3. Results and discussion

In this study, we demonstrated a novel method to: (1) reconstruct time-series shelf-based 3D meshes for a NAM population of Arabidopsis with a stationary multi-camera array imaging system in a controlled environment, (2) capture time-series of 2D rosette areas for studying plant nastic movements and diurnal

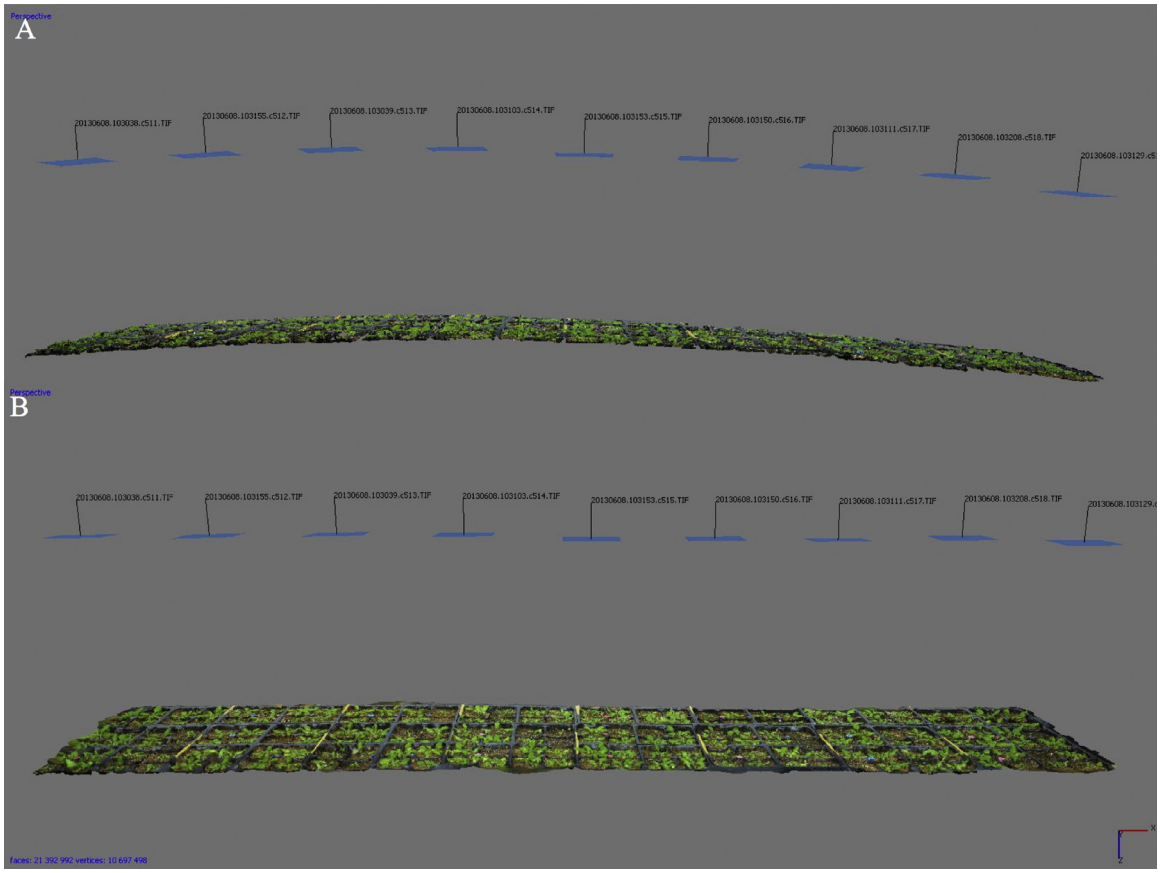

Fig. 8. Half-shelf 3D mesh before and after camera calibration. A) The half-shelf 3D mesh showed curvature before camera calibration. No plant area could be estimated at this point. B) The same model with accurate camera intrinsic parameters; the 3D mesh was flat.

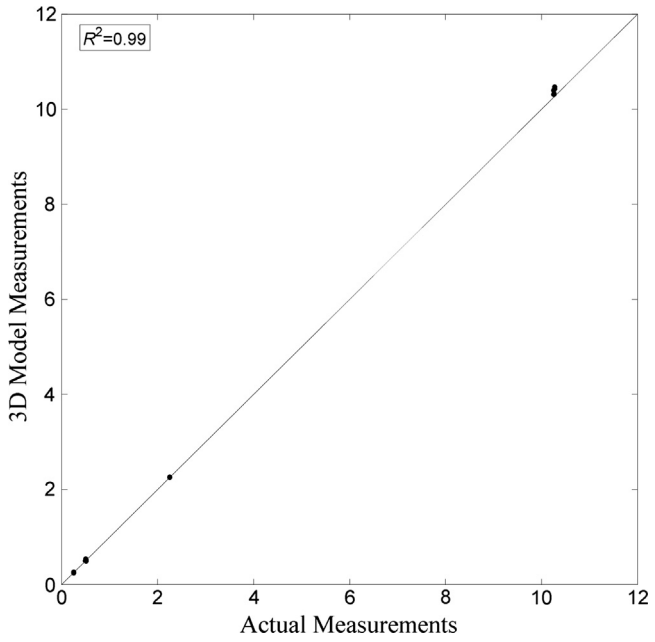

Fig. 9. 3D measurement accuracy test. Accuracy test of the 3D measurements. X-axis is the actual physical size of the objects and y-axis is the measurements from the 3D meshes. The R square is 0.99 and the slope of the linear regression is 1.01.

cycles, (3) extract single-plant 3D models from background 3D mesh, (4) assign genotypic information to replicate plants, and (5) compute time-series 3D areas during a 10-day growth period. This process was integrated into our high-throughput phenotyping pipeline in order to automate extraction of 3D plant phenotypic traits. These methods enable phenotyping throughput needed for genomic mapping studies, and we anticipate they could be translated to other morphological phenotypes of interested.

3.1. Camera array calibration and measurement accuracy test

Few previous studies have taken camera intrinsic parameters into account when using digital cameras for plant phenotyping, which could greatly reduce image-based phenotypic measurement accuracy. An et al. (2016) demonstrated that camera calibration is a critical step to enhance accuracy before using images to quantify plant phenotypes. Fig. 8A shows the 3D modeling results before camera calibration. Due to the linear camera array setup, the intrinsic parameters could not be estimated accurately by Photoscan because no information was available from other viewpoints. Without correct camera intrinsic parameters, both the one-row camera array and the half-shelf 3D mesh showed curvature. The lack of information arose because there was not enough vertical clearance for the fields of view of cameras in separate rows to overlap when plants were present. To ensure effective camera array calibration, the field of view of the camera arrays should ensure

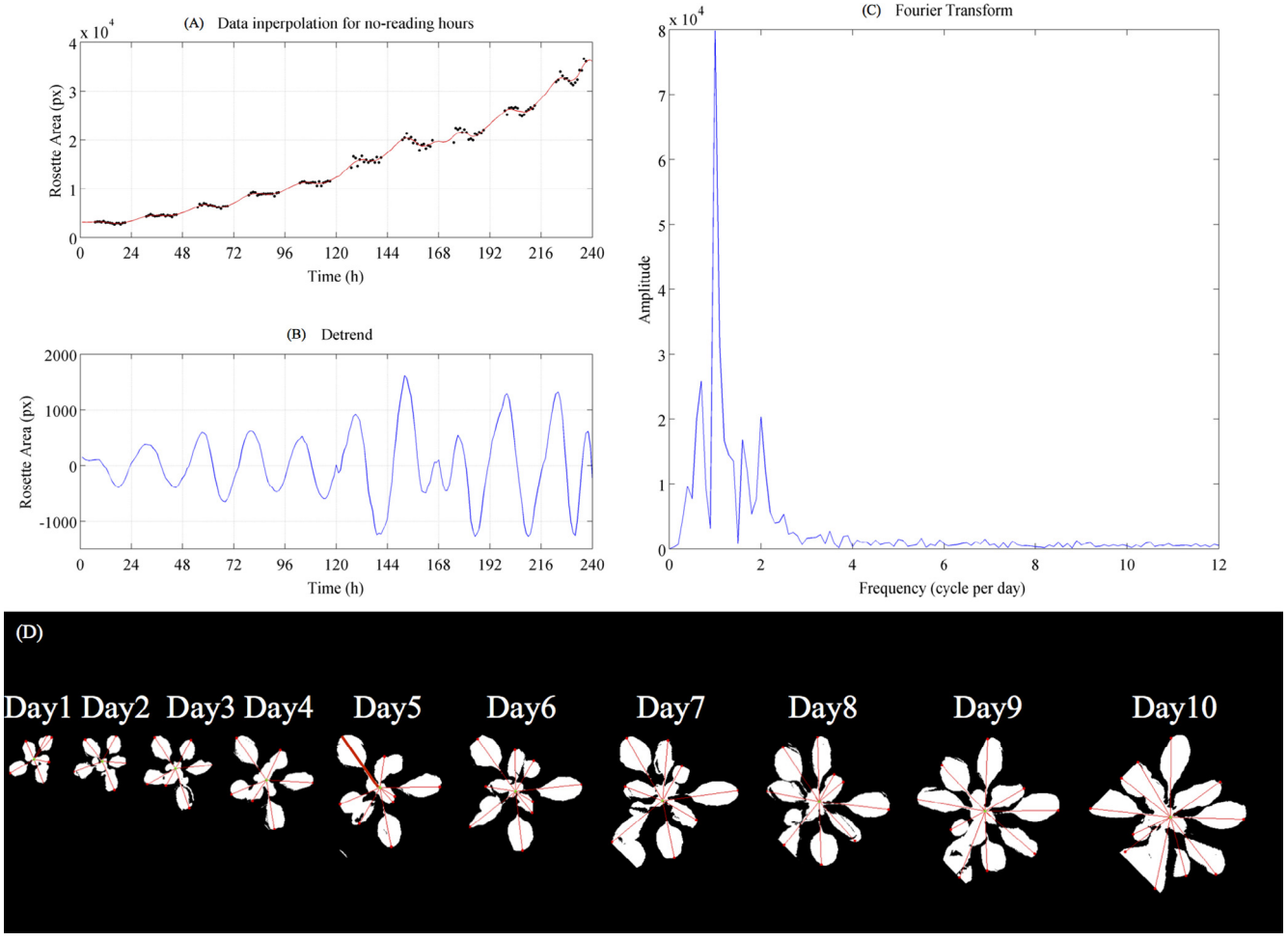

Fig. 10. Plant nastic movement and diurnal cycle analysis. (A) The graph is the 16-h rosette area measurements (black dots) and smoothed growth curve (red curve); (B) the detrended plant growth curve to show the plant nastic movement; (C) the Fourier Transform to the diurnal movement is a daily cycle; (D) time-series 2D single-rosette binary images for this plant. (For interpretation of the references to color in this figure legend, the reader is referred to the web version of this article.)

at least 50% overlap between rows of cameras, that is, experimental plants are in the field of view two cameras.

Before the pots were placed on the shelf surface, the vertical space was sufficient for Photoscan to group both rows of cameras together for camera intrinsic parameter estimation. By using the camera intrinsic parameters estimated by the calibration, both the one-row camera array and the half-shelf 3D mesh are flat and the estimation errors were less than 0.5 pixels, as Fig. 8B shows. Comparing the studies (Quan et al., 2006; Tan et al., 2007; Biskup et al., 2007; Santos and Oliveira 2012) introduced previously, our 3D imaging system can quantify high-accuracy 3D plant models with much higher throughput for a large number of plants in a mapping populations.

Due to space limitations and an attendant limit on the number of replicate plants that could be grown at one time, it was not feasible to carry out destructive harvests and collect direct rosette area measurements to validate the modeled 3D rosette area. In principle, the model accuracy could be tested by comparing the physical size of objects to the measurements on 3D mesh. For the accuracy test in this study, a scale factor was first determined by computing the ratio of the physical sizes of the color grids on the poster and the measurements on 3D mesh of the poster model. This scale factor was then used to translate the half-shelf 3D plant models from 3D units to a scientific units. The physical sizes of ten small color dots, ten large color dots, ten pots and ten 4-pot by 4-pot trays of each shelf were measured, and those objects were

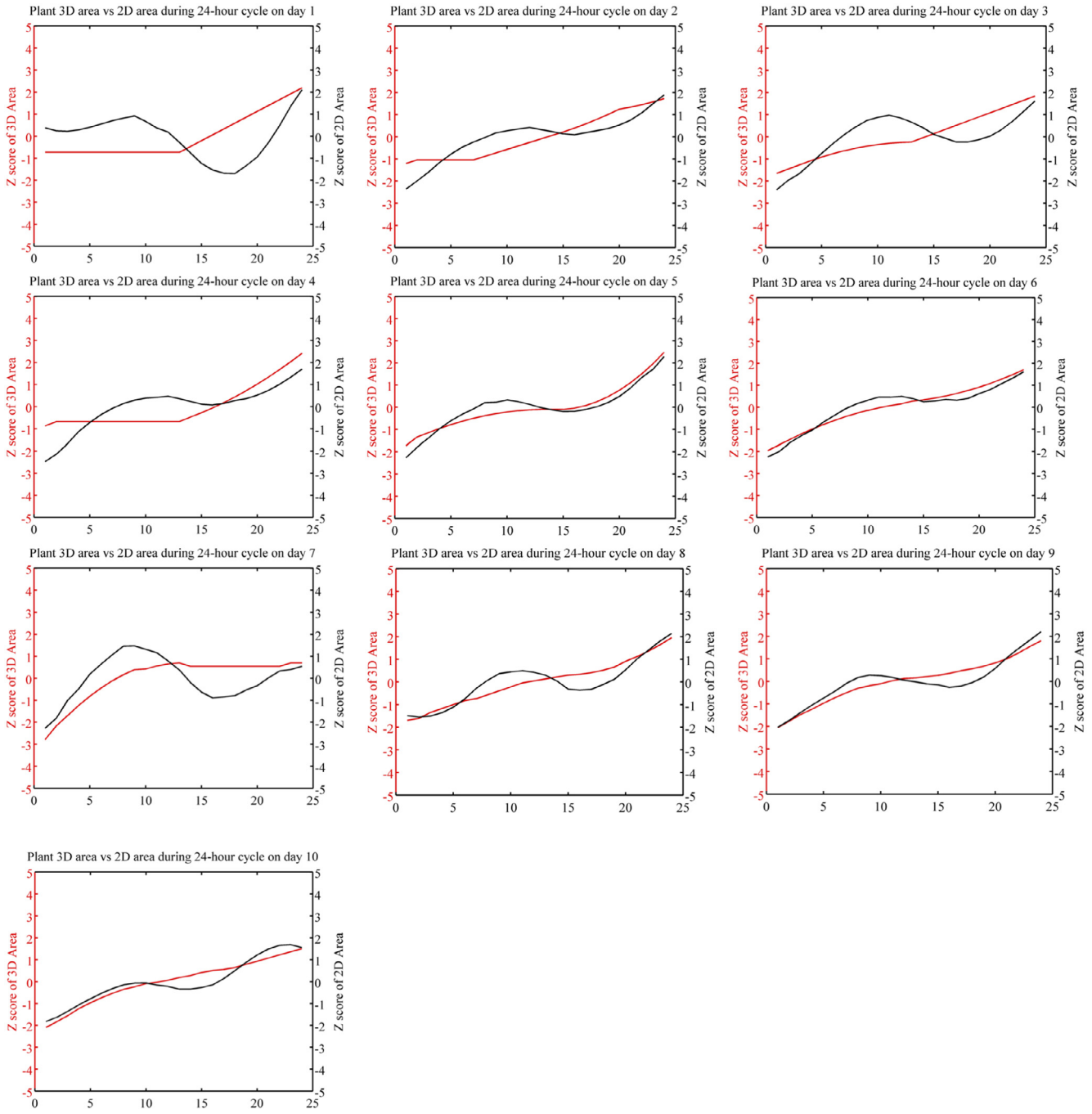

Fig. 11. Z score comparison between 3D area and 2D area. Daily Z scores comparisons between 3D areas (red curve) and 2D areas (black curve) during a 10-day growth period. (For interpretation of the references to color in this figure legend, the reader is referred to the web version of this article.)

also measured from 3D meshes. The slope of the linear regression was 1.01 and the R square was 0.99, demonstrating that accurate plant measurements could be extracted from the 3D mesh (Fig. 9).

3.2. Plant nastic movement and diurnal cycle analysis

The black dots in Fig. 10A are the actual time-series 2D rosette area measurements, and the red curve is the smoothed 2D rosette area curve after interpolation for night-time data. The oscillation caused by plant nastic movement in the red curve is visible but is distorted by the overall pattern of increasing size that will also affect the Fourier Transform results. There is noticeable noise at Day 4, Day 6 and Day 8 in Fig. 10A. This likely arises from pot rotation, which took place every other day and was used to randomize microenvironmental variation in the growth chamber across replicates plants. After detrending the 2D rosette area curve (Fig. 10B), the daily time at which this plant reaches its maximum apparent area is between 9:00 am (ZT4) and 10:00 am (ZT5). Furthermore, the oscillation is more obvious than without curve detrending. The peak of the Fourier Transform (Fig. 10C) is at a 24-h frequency. This result is similar to previous studies (Hong et al., 2013; Dornbusch et al., 2014; Greenham et al., 2015) and shows that our automated pipeline can extract diurnal patterns. Fig. 10D shows the overall daily growth of the plant. The individual leaf pictures were taken at 6:00 am (ZT1) each day, when the leaves were almost horizontal. Fig. 10D shows rosette leaves with seemingly straight edges. This leaf shape distortion arises from rosette overlap between adjacent experimental plants. Leaf overlap was discernible by Day 10, potentially leading to inaccurate 2D rosette area measurements; measurements therefore stopped at Day 10.

3.3. Time-series comparison between 2D area and 3D area

Fig. 11 superimposes the day-by-day Z score plots, directly comparing the 2D (black curve) and 3D (red curve) areas. Across the 10-day growth period, the 3D areas mainly show slow linear growth trends within each day and lack the oscillations caused by plant nastic movement in 2D areas. Also, the starting and ending measurements for both 2D and 3D curves are very close to one another within each day at times when the leaves are closest to horizontal.

Comparing the plants' areas as measured from the 3D model and a corresponding 2D image during a 10-day growth period showed that both approaches captured increasing leaf areas, but that the 3D data was uncorrupted by plant nastic movements. This result shows that areas measured in a 3D space might be more accurate and reliable when modeling and analyzing biological growth responses. Furthermore, 3D plant models can provide a unique perspective to study plant canopy structure and plant growth patterns under different environmental conditions with non-invasive and non-destructive sampling methods.

3.4. Single-plant 3D modeling pipeline throughput

The processing pipeline has very high imaging and measurement throughput for 3D and 2D plant areas. For each half-shelf, it took approximately 35 min for image pre-processing, orthophoto generation, 3D mesh reconstruction, binary image segmentation, and genotype assignment, as a result of GPU acceleration with OpenCL. However, once the 3D mesh is stored in the system memory, it only takes 3.84 s to process the half-shelf 3D mesh. In other words, it took 0.02 s on an Intel Core i7 processor to extract a single-plant 3D model from the half-shelf 3D mesh. For each plant, it took approximately 3.2 s to compute hourly 2D and 3D areas during a 10-day growth period (total: 160 plants). This improvement allowed us to screen 1050 plants within 50 s for their 2D and 3D areas, which has not been accomplished previously by relatively low-cost imaging systems.

4. Conclusion and perspectives

In this study, we presented novel photogrammetry and computer vision algorithms to quantify leaf morphological traits, 2D and 3D leaf areas, and diurnal cycles of leaf movement with relatively low-cost imaging systems. Such systems could provide high-accuracy 3D canopy models for large mapping populations of Arabidopsis with very high throughput: the processing time for single-plant 3D model extraction and 3D area calculation was extremely fast (0.02 s per plant) after applying optimized algorithms. The high-throughput phenotyping pipeline presented in this study showed significant potential for large-scale noninvasive plant measurement. This not only supports improved understanding of plant growth and development in a time-series manner but also can help determine the performance of specific genotypes by analyzing whole-plant phenotypic traits. The current limitation is the runtime for generating and reading the 3D canopy models; the runtime is approximately 35 min due to the large number of vertices and faces of each half-shelf mesh. For future work, the camera array step should be redesigned so that an entire shelf of plants is imaged with grouped two-row camera systems. A further investigation on how to optimize the runtime for reading half-shelf mesh is needed in order to improve current processing throughput. Leaf morphological traits, such as leaf length measured in the three-dimensional space, may be quantified as a comparison to 2D leaf length.

Acknowledgement

This study was funded by the National Science Foundation Grant IOS-0923752 to Cynthia Weinig, Stephen Welch, and Julin Maloof. RJC Markelz was supported by a National Science Foundation Postdoctoral Fellowship in Biology IOS-1402495.

References

Ali, M.M., Al-Ani, A., Eamus, D., Tan, D.K., 2012. A new image-processing-based technique for measuring leaf dimensions. Am.–Eurasian J. Agric. Environ. Sci. 12, 1588–1594.

An, N., Palmer, C.M., Baker, R.L., Markelz, R.J.C., Ta, J., Covington, M.F., Maloof, J.N., Welch, S.M., Weinig, C., 2016. Plant High-Throughput Phenotyping Using Photogrammetry and Imaging Techniques to Measure Leaf Length and Rosette Area. Comput. Electron. Agric. 127 (2016), 376–394.

Azzari, G., Goulden, M.L., Rusu, R.B., 2013. Rapid characterization of vegetation structure with a microsoft kinect sensor. Sensors 13 (2), 2384–2398.

Backhaus, A., Kuwabara, A., Bauch, M., Monk, N., Sanguinetti, G., Fleming, A., 2010. LEAFPROCESSOR: a new leaf phenotyping tool using contour bending energy and shape cluster analysis. New Phytol. 187 (1), 251–261.

Berger, B., Parent, B., Tester, M., 2010. High-throughput shoot imaging to study drought responses. J. Exp. Bot. erq201.

Bellasio, C., Olejníčková, J., Tesař, R., Šebela, D., Nedbal, L., 2012. Computer reconstruction of plant growth and chlorophyll fluorescence emission in three spatial dimensions. Sensors 12 (1), 1052–1071.

Biskup, B., Scharr, H., Schurr, U., Rascher, U.W.E., 2007. A stereo imaging system for measuring structural parameters of plant canopies. Plant, Cell Environ. 30 (10), 1299–1308.

Brachi, B., Faure, N., Horton, M., Flahauw, E., Vazquez, A., Nordborg, M., Bergelson, J., Cuguen, J., Roux, F., 2010. Linkage and association mapping of Arabidopsis thaliana flowering time in nature. PLoS Genet. 6 (5), e1000940. http://dx.doi.org/10.1371/journal.pgen.1000940.

Bylesjö, M., Segura, V., Soolanayakanahally, R.Y., Rae, A.M., Trygg, J., Gustafsson, P., Jansson, S., Street, N.R., 2008. LAMINA: a tool for rapid quantification of leaf size and shape parameters. BMC Plant Biol. 8 (1), 82.

Candela, H., Martınez-Laborda, A., Micol, J.L., 1999. Venation pattern formation in Arabidopsis thaliana vegetative leaves. Dev. Biol. 205 (1), 205–216.

Chen, D., Neumann, K., Friedel, S., Kilian, B., Chen, M., Altmann, T., Klukas, C., 2014. Dissecting the phenotypic components of crop plant growth and drought responses based on high-throughput image analysis. Plant Cell 26 (12), 4636–4655.

Chéné, Y., Rousseau, D., Lucidarme, P., Bertheloot, J., Caffier, V., Morel, P., Belin, É., Chapeau-Blondeau, F., 2012. On the use of depth camera for 3D phenotyping of entire plants. Comput. Electron. Agric. 82, 122–127.
Clarke, J.H., Mithen, R., Brown, J.K., Dean, C., 1995. QTL analysis of flowering time in Arabidopsis thaliana. Mol. Gen. Genet. (MGG) 248 (3), 278–286.
Dornbusch, T., Michaud, O., Xenarios, I., Fankhauser, C., 2014. Differentially phased leaf growth and movements in Arabidopsis depend on coordinated circadian and light regulation. Plant Cell 26 (10), 3911–3921.
Easlon, H.M., Bloom, A.J., 2014. Easy leaf area: automated digital image analysis for rapid and accurate measurement of leaf area. Appl. Plant Sci. 2 (7).
El-Omari, S., Moselhi, O., 2011. Integrating automated data acquisition technologies for progress reporting of construction projects. Autom. Constr. 20 (6), 699–705.
Fiorani, F., Schurr, U., 2013. Future scenarios for plant phenotyping. Annu. Rev. Plant Biol. 64, 267–291.
Furbank, R.T., Tester, M., 2011. Phenomics–technologies to relieve the phenotyping bottleneck. Trends Plant Sci. 16 (12), 635–644.
Granier, C., Aguirrezabal, L., Chenu, K., Cookson, S.J., Dauzat, M., Hamard, P., Thioux, J., Rolland, G., Bouchier-Combaud, S., Lebaudy, A., Muller, B., Simonneau, T., Tardieu, F., 2006. PHENOPSIS, an automated platform for reproducible phenotyping of plant responses to soil water deficit in Arabidopsis thaliana permitted the identification of an accession with low sensitivity to soil water deficit. New Phytol. 169 (3), 623–635.
Green, J.M., Appel, H., Rehrig, E.M., Harnsomburana, J., Chang, J.F., Balint-Kurti, P., Shyu, C.R., 2012. PhenoPhyte: a flexible affordable method to quantify 2D phenotypes from imagery. Plant Methods 8 (1), 1–12.
Greenham, K., Lou, P., Remsen, S.E., Farid, H., McClung, C.R., 2015. TRiP: Tracking Rhythms in Plants, an automated leaf movement analysis program for circadian period estimation. Plant Methods 11 (1), 33.
Hartmann, A., Czauderna, T., Hoffmann, R., Stein, N., Schreiber, F., 2011. HTPheno: an image analysis pipeline for high-throughput plant phenotyping. BMC Bioinf. 12 (1), 148.
Hosoi, F., Omasa, K., 2009. Estimating vertical plant area density profile and growth parameters of a wheat canopy at different growth stages using three-dimensional portable lidar imaging. ISPRS J. Photogram. Remote Sens. 64 (2), 151–158.
Hong, S., Kim, S.A., Guerinot, M.L., McClung, C.R., 2013. Reciprocal interaction of the circadian clock with the iron homeostasis network in Arabidopsis. Plant Physiol. 161 (2), 893–903.
Hunt Jr., E.R., Cavigelli, M., Daughtry, C.S., Mcmurtrey III, J.E., Walthall, C.L., 2005. Evaluation of digital photography from model aircraft for remote sensing of crop biomass and nitrogen status. Precis. Agric. 6 (4), 359–378.
Juenger, T.E., Mckay, J.K., Hausmann, N., Keurentjes, J.J., Sen, S., Stowe, K.A., Dawson, T.E., Simms, E.L., Richards, J.H., 2005. Identification and characterization of QTL underlying whole-plant physiology in Arabidopsis thaliana: $\delta^{13}C$, stomatal conductance and transpiration efficiency. Plant, Cell Environ. 28 (6), 697–708.
Keightley, K.E., Bawden, G.W., 2010. 3D volumetric modeling of grapevine biomass using Tripod LiDAR. Comput. Electron. Agric. 74 (2), 305–312.
Kjaer, K.H., Ottosen, C.O., 2015. 3D laser triangulation for plant phenotyping in challenging environments. Sensors 15 (6), 13533–13547.
Mahlein, A.K., Oerke, E.C., Steiner, U., Dehne, H.W., 2012. Recent advances in sensing plant diseases for precision crop protection. Eur. J. Plant Pathol. 133 (1), 197–209.
Maloof, J.N., Nozue, K., Mumbach, M.R., Palmer, C.M., 2013. LeafJ: an ImageJ plugin for semi-automated leaf shape measurement. J. Visual. Exp. 71, pp. e50028–e50028.
Mullen, J.L., Weinig, C., Hangarter, R.P., 2006. Shade avoidance and the regulation of leaf inclination in Arabidopsis. Plant, Cell Environ. 29 (6), 1099–1106.
Palacín, J., Pallejà, T., Tresanchez, M., Sanz, R., Llorens, J., Ribes-Dasi, M., Masip, J., Arnó, J., Escolà, A., Rosell, J.R., 2007. Real-time tree-foliage surface estimation using a ground laser scanner. IEEE Trans. Instrum. Meas. 56 (4), 1377–1383.
Paulus, S., Behmann, J., Mahlein, A.K., Plümer, L., Kuhlmann, H., 2014. Low-cost 3D systems: suitable tools for plant phenotyping. Sensors 14 (2), 3001–3018.
Pérez-Pérez, J.M., Serrano-Cartagena, J., Micol, J.L., 2002. Genetic analysis of natural variations in the architecture of Arabidopsis thaliana vegetative leaves. Genetics 162 (2), 893–915.
Quan, L., Tan, P., Zeng, G., Yuan, L., Wang, J., Kang, S.B., 2006. Image-based plant modeling. In: ACM Transactions on Graphics (TOG), 25(3). ACM, pp. 599–604.
Rascher, U., Blossfeld, S., Fiorani, F., Jahnke, S., Jansen, M., Kuhn, A.J., Matsubara, S., Märtin, L.L.A., Merchant, A., Metzner, R., Müller-Linow, M., Nagel, K.A., Pieruschka, R., Pinto, F., Schreiber, C.M., Temperton, V.M., Thorpe, M.R., Dusschoten, D.V., Volkenburgh, E.V., Windt, C.W., Schurr, U., 2011. Non-invasive approaches for phenotyping of enhanced performance traits in bean. Funct. Plant Biol. 38 (12), 968–983.
Santos, T.T., Oliveira, A.A., 2012. Image-based 3D digitizing for plant architecture analysis and phenotyping. In: Workshop on Industry Applications (WGARI) in SIBGRAPI 2012. pp. 21–28.
Tan, P., Zeng, G., Wang, J., Kang, S.B., Quan, L., 2007. Image-based tree modeling. In: ACM Transactions on Graphics (TOG), 26(3). ACM, pp. 87–604.
Vos, J., Evers, J.B., Buck-Sorlin, G.H., Andrieu, B., Chelle, M., De Visser, P.H., 2009. Functional–structural plant modelling: a new versatile tool in crop science. J. Exp. Bot., erp345
Weight, C., Parnham, D., Waites, R., 2008. TECHNICAL ADVANCE: LeafAnalyser: a computational method for rapid and large-scale analyses of leaf shape variation. Plant J. 53 (3), 578–586.